ARMY RESEARCH LABORATORY

Aero-Elastic Motion of a Spin-Stabilized Projectile

by Charles H. Murphy and William H. Mermagen, Sr.

ARL-TR-3453 **March 2005**

NOTICES

Disclaimers

The findings in this report are not to be construed as an official Department of the Army position unless so designated by other authorized documents.

Citation of manufacturer's or trade names does not constitute an official endorsement or approval of the use thereof.

Destroy this report when it is no longer needed. Do not return it to the originator.

Army Research Laboratory
Aberdeen Proving Ground, MD 21005-5066

ARL-TR-3453 **March 2005**

Aero-Elastic Motion of a Spin-Stabilized Projectile

Charles H. Murphy and William H. Mermagen, Sr.
Weapons and Materials Research Directorate, ARL

REPORT DOCUMENTATION PAGE

Form Approved
OMB No. 0704-0188

1. REPORT DATE *(DD-MM-YYYY)*	2. REPORT TYPE	3. DATES COVERED (From - To)
March 2005	Final	October 2003-April 2004

4. TITLE AND SUBTITLE
Aero-Elastic Motion of a Spin-Stabilized Projectile

5a. CONTRACT NUMBER

5b. GRANT NUMBER

5c. PROGRAM ELEMENT NUMBER

6. AUTHOR(S)
Charles H. Murphy and William H. Mermagen, Sr.

5d. PROJECT NUMBER
AH 80

5e. TASK NUMBER

5f. WORK UNIT NUMBER

7. PERFORMING ORGANIZATION NAME(S) AND ADDRESS(ES)
U.S. Army Research Laboratory
ATTN: AMSRD-ARL-WM-BC
Aberdeen Proving Ground, MD 21005-5066

8. PERFORMING ORGANIZATION REPORT NUMBER
ARL-TR-3453

9. SPONSORING/MONITORING AGENCY NAME(S) AND ADDRESS(ES)

10. SPONSOR/MONITOR'S ACRONYM(S)

11. SPONSOR/MONITOR'S REPORT NUMBER(S)

12. DISTRIBUTION/AVAILABILITY STATEMENT
Approved for public release; distribution is unlimited.

13. SUPPLEMENTARY NOTES

14. ABSTRACT
The elastic flight motion of a slowly spinning finned missile has been successfully described by the finite element method (FEM). With the addition of a Magnus force distribution function, this analysis was used to describe the elastic flight motion of a spin-stabilized projectile. Transient frequencies and damping rates for a 10-cal. cone cylinder have been calculated. The elastic frequencies for a rapidly spinning projectile can be substantially different from those for zero spin. A slightly bent projectile can have a large deflection when its spin rate is near an elastic frequency. Resonant motion is demonstrated when the spin is near the first positive elastic frequency. The maximum strain associated with this motion can exceed the plastic limit.

15. SUBJECT TERMS
aero-elasticity, FEM, symmetric missile

16. SECURITY CLASSIFICATION OF:			17. LIMITATION OF ABSTRACT	18. NUMBER OF PAGES	19a. NAME OF RESPONSIBLE PERSON
a. REPORT	b. ABSTRACT	c. THIS PAGE			Charles H. Murphy
UNCLASSIFIED	UNCLASSIFIED	UNCLASSIFIED	UL	40	19b. TELEPHONE NUMBER (*Include area code*) 410-278-3684

Standard Form 298 (Rev. 8/98)
Prescribed by ANSI Std. Z39.18

Contents

List of Figures iv

List of Tables iv

1. Introduction 1

2. Coordinate System 1

3. Aerodynamic Force 3

4. Frequencies 5

5. FEM 7

6. Cone Cylinder Frequencies 8

7. Bent Projectile Resonances 9

8. Summary 14

9. References 15

Appendix A. Improved Partial Differential Equation 17

Appendix B. Integrals 21

Appendix C. Magnus Terms 23

Appendix D. Projectile Parameters 25

List of Symbols, Abbreviations, and Acronyms 27

Distribution List 30

List of Figures

Figure 1. *X-Z* coordinates of the cross-sectional disk. 2
Figure 2. *X-Y* coordinates of the cross-sectional disk. 3
Figure 3. Shape of the beam for *j* = 3, 5, 7 element and PDE (real part of the shape). 9
Figure 4. $\dot{\phi}_3/\omega_1, -\dot{\phi}_4/\omega_1$ vs. σ. 10
Figure 5. $\dot{\phi}_5/\omega_2, -\dot{\phi}_6/\omega_2$ vs. σ. 10
Figure 6. $mag(s_{11})$ vs. σ for 5-element code, $\dot{\phi}$ = 7200 rad/s, 6800 rad/s. 11
Figure 7. $\dot{\phi}$ vs. time for σ = 122.8, $\dot{\phi}_0$ = 7100. 12
Figure 8. $mag(q_{1b})$ vs. time for σ = 122.8, $\dot{\phi}_0$ = 7100. 13
Figure 9. $mag(q_{11b})$ vs. time for σ = 122.8, $\dot{\phi}_0$ = 7100. 13
Figure 10. mag (e_M) vs. time for σ = 122.8, $\dot{\phi}_0$ = 7100. 14

List of Tables

Table D-1. Transient frequencies and damping rates. 26

1. Introduction

The free-flight motion of a slowly spinning elastic missile has been studied by a number of authors (*1–6*). Although the theory of Murphy and Mermagen (*6*) is valid for large spin rates, no Magnus force is included in the aerodynamic force distribution. In this report, the force distribution is extended to include a Magnus force distribution function. The finite element method (FEM) (*6*) is then used to calculate the first five positive frequencies and the first three negative frequencies of the motion of a 10-cal. spinning cone cylinder. The elastic frequencies are shown to be strongly affected by the high rate of spin required to stabilize this projectile. For certain values of the elasticity, it is shown that spin resonance can occur with the lower elastic positive frequencies, and maximum strain can exceed the plastic limit.

2. Coordinate System

The elastic missile is assumed to consist of a very heavy elastic circular rod of fineness ratio, L, and mass, m, embedded in a very light symmetric aerodynamic structure that may be longer than the rod. The rod's axial moment of inertia is I_x, and its transverse moment of inertia about its center is I_{t0}. The rod's diameter can vary over its length, and its maximum diameter will be denoted by d. All distances will be expressed as multiples of the rod diameter, and its length is Ld. A nose windshield of length, $x_{23}d$, may be attached to the forward end of the rod, and fins or a boat tail may extend beyond the end of the rod at a distance, $x_{01}d$. Thus, the rod is located between $x_1 = -L/2$ and $x_2 = L/2$, while the aerodynamic structure extends from $x_0 = x_1 - x_{01}$ to $x_3 = x_2 + x_{23}$.

An earth-fixed coordinate system will be used with the X_e-axis oriented along the initial direction of the missile's velocity vector. The Z_e-axis is downward pointing and the Y_e-axis determined by the right hand rule. A nonrotating coordinate system, XYZ is then defined with origin always at the center of the rod and the X-axis tangent there. The X-axis pitches through the angle, θ, and yaws through the angle, ψ, with respect to the X_e-axis. Body-fixed coordinates, XY_bZ_b, are now defined for which the Y_b-Z_b axes rotate with the missile.

We will conceptually slice the missile into a large number of thin disks perpendicular to the X-axis with thickness, dx. When the rod flexes, the disks shift laterally perpendicular to the X-axis and cant to be perpendicular to the centerline of the disks. This canting action neglects the shear deformation of the rod, and this constraint is called the Bernoulli assumption (*7*). The lateral displacement of a disk has body-fixed coordinates δ_{by}, δ_{bz}, and the disk is canted at angles Γ_{by}, Γ_{bz}.

$$\Gamma_{by} = \frac{\partial \delta_{by}}{\partial x}; \qquad \Gamma_{bz} = \frac{\partial \delta_{bz}}{\partial x} \tag{1}$$

It is important to note that at the central disk

$$\delta_{by}(0,t) = \delta_{bz}(0,t) = \Gamma_{by}(0,t) = \Gamma_{bz}(0,t) = 0\,. \tag{2}$$

The earth-fixed coordinates of the central disk are (x_e, y_e, z_e), and the earth-fixed coordinates of the other disks are computed in terms of the central disk earth-fixed coordinates, their body-fixed displacements, and the Euler angles θ, ψ, ϕ:

$$x_{de} = x_e + x\left[1 - \left(\psi^2 + \theta^2\right)/2\right] - \psi Re\left\{\left(\delta_{by} + i\delta_{bz}\right)e^{i\phi}\right\} + \theta Im\left\{\left(\delta_{by} + i\delta_{bz}\right)e^{i\phi}\right\}, \tag{3}$$

$$y_{de} = y_e + x\psi + Re\left\{\left(\delta_{by} + i\delta_{bz}\right)e^{i\phi}\right\}, \tag{4}$$

and

$$z_{de} = z_e - x\theta + Im\left\{\left(\delta_{by} + i\delta_{bz}\right)e^{i\phi}\right\}. \tag{5}$$

Murphy and Mermagen (*5*, *6*) used the nonspinning elastic coordinate system with *XYZ* axes. $(\phi = 0)$. The lateral displacements of a disk in this elastic coordinate system are shown in figures 1 and 2 and can be computed from body-fixed quantities.

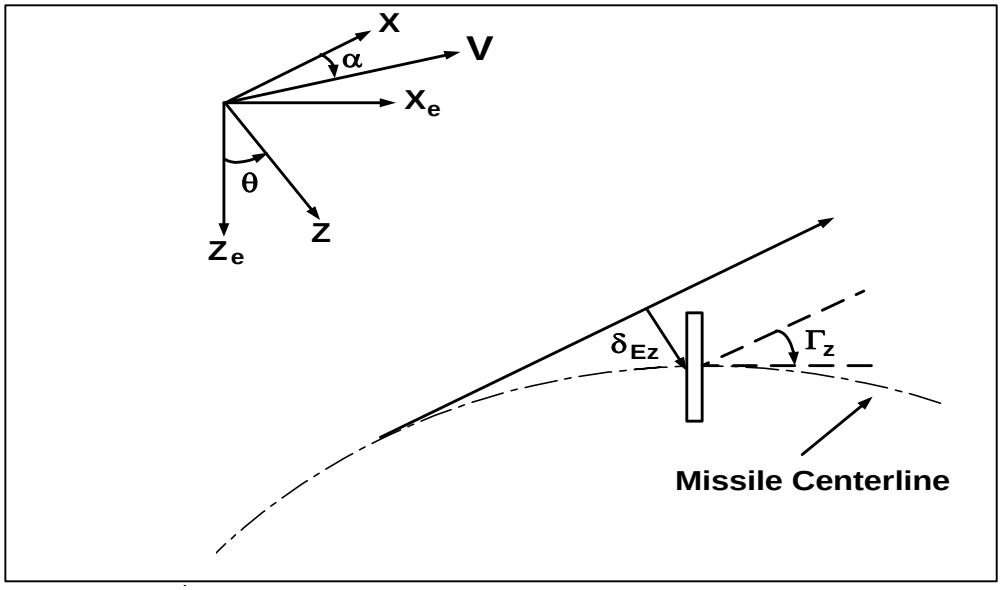

Figure 1. *X-Z* coordinates of the cross-sectional disk.

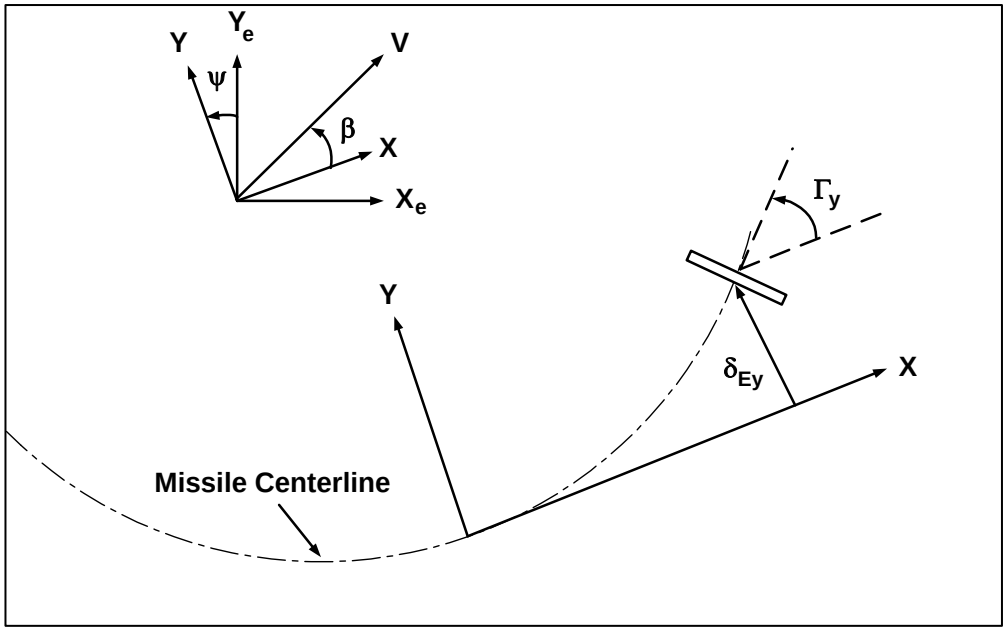

Figure 2. *X-Y* coordinates of the cross-sectional disk.

$$\delta_E = \delta_{Ey} + i\delta_{Ez} = \left(\delta_{by} + i\delta_{bz}\right)e^{i\phi}, \tag{6}$$

and

$$\Gamma = \Gamma_y + i\Gamma_z = \left(\Gamma_{by} + i\Gamma_{bz}\right)e^{i\phi}. \tag{7}$$

In Murphy and Mermagen (*5*), the partial differential equation (PDE) for the missile's flexing motion is derived by use of Newtonian mechanics and the assumption that each disk can be assumed to be a point mass. Thus, the canting of the disks is neglected, and their axial and transverse moments of inertia are set equal to zero. The complete Lagrangian is obtained including the canting of the disks required by the Bernoulli assumption and is used to obtain a more accurate PDE in appendix A. For the small spin considered, this modification has a very small effect on the eigenfrequencies. For a spin-stabilized projectile, the required spin can be 30–100 times the aerodynamic frequencies and can have a large effect on the eigenfrequencies.

3. Aerodynamic Force

The y_e and z_e components of the central disk velocity can be approximated by linear relations in angles of pitch and yaw with respect to inertia axes (θ, ψ) and angles of attack and sideslip with respect to the velocity vector (α, β) (figures 1 and 2).

$$\dot{y}_e = (V/d)(\beta + \psi), \tag{8}$$

and

$$\dot{z}_e = (V/d)(\alpha - \theta). \tag{9}$$

Equations 8 and 9 can be written as a single complex equation:

$$\dot{y}_e + i\dot{z}_e = (V/d)(q_1 + q_{1e}), \tag{10}$$

where

$$q_1 = \beta + i\alpha \tag{11}$$

and

$$q_{1e} = \psi - i\theta. \tag{12}$$

In Murphy and Mermagen (*5*), the linear aerodynamic force loading is expressed in terms of three force distribution functions, $c_D(x), c_{f1}(x), c_{f2}(x)$ and the base pressure coefficient, C_{Dbp}, plus a body-fixed force associated with possible bent fins. The complex angular velocity of the central disk is $q_2 = \dot{q}_{1e}$. Because the lateral motion of the missile is quite small, $\dot{q}_1 \cong -q_2$, and the aerodynamic damping force terms in the aerodynamic loading on the aerodynamic structure can be combined. For a rapidly spinning projectile, we will introduce a Magnus force distribution function $c_{fM}(x)$. This aerodynamic loading in nonrotating elastic coordinates is

$$\frac{dF_x}{dx} = -g_1 c_D(x). \tag{13}$$

$$\frac{dF_y}{dx} + i\frac{dF_z}{dx} = -g_1 \left[\begin{array}{c} \left[c_{f1}(x) + i\left(\dot{\phi}d/V\right) c_{fM}(x) \right] \left[q_1 - \Gamma + \left(\dot{\delta}_E - x\dot{q}_1\right)(d/V) \right] \\ + c_{f2}(x)\left(2\dot{q}_1 - \dot{\Gamma}\right)(d/V) \end{array} \right]. \tag{14}$$

$$F_{xbp} = -g_1 C_{Dbp}. \tag{15}$$

The total aerodynamic force acting on the aerodynamic structure is given by the integrals of equations 13 and 14 and by adding the base drag of equation 15 to the axial force:

$$F_x = -g_1 C_D = -g_1 \left[\int_{x_0}^{x_3} c_D(x)\, dx + C_{Dbp} \right], \tag{16}$$

and

$$F = -g_1 \left[\begin{array}{l} \left(c_1 + i\left(\dot{\phi}d/V\right) c_{1M}\right) q_1 + c_2\left(\dot{q}_1 d/V\right) \\ -J_1(t) - i\left(\dot{\phi}d/V\right) J_{1M}(t) - \dot{J}_2(t)(d/V) \end{array} \right], \tag{17}$$

where various functions are defined in appendix B.

Similarly, the transverse aerodynamic moment about the rod's center can be computed from the transverse aerodynamic force and a small axial force contribution:

$$\begin{aligned} M &= M_y + iM_z \\ &= -i\left(g_1 d\right)\begin{bmatrix} \left(c_3 + i\left(\dot{\phi}d/V\right)c_{3M}\right)q_1 + c_4\left(\dot{q}_1 d/V\right) \\ -J_3(t) - i\left(\dot{\phi}d/V\right)J_{3M}(t) - \dot{J}_4(t)\left(d/V\right) - J_5(t) \end{bmatrix}. \end{aligned} \tag{18}$$

The primary components of drag are head drag and base pressure drag. The third component is skin friction drag that is ~15% of the total drag and will be neglected in this report to simplify the FEM calculations.

The actual angular motion will be described by aerodynamic moment about the center of mass. The static and Magnus moment coefficients, for example, are as follows:

$$C_{M\alpha} = c_3 - x_c c_1, \tag{19}$$

and

$$C_{Mp\alpha} = c_{3M} - x_c c_{1M}, \tag{20}$$

where

$$x_c = \left(1/L\right)\int_{x_1}^{x_2} x\rho_1 dx. \tag{21}$$

The center of mass of the projectile will be at the center of the rod if the axial mass density along the rod, ρ_1, is constant.

4. Frequencies

For simplicity, the spin will be required to be always positive. The angular motion of a statically stable rigid missile ($C_{M\alpha} < 0$) can be described by the sum of two complex exponentials:

$$q_1 = K_{10}e^{\left(\lambda_1 + i\dot{\phi}_{1R}\right)t} + K_{20}e^{\left(\lambda_2 + i\dot{\phi}_{2R}\right)t}, \tag{22}$$

where

$$\dot{\phi}_{mR} = \dot{\phi}I_x/2I_t \pm \sqrt{-\left(g_1 d/I_t\right)C_{M\alpha}\left(1 - s_g\right)} \tag{23}$$

and

$$s_g = \frac{\dot{\phi}^2 I_x^2}{I_t g_1 d C_{M\alpha}}. \tag{24}$$

These two frequencies are opposite in sign and $\left|\dot{\phi}_{1R}\right| \geq \left|\dot{\phi}_{2R}\right|$. The motion of a statically unstable missile ($C_{M\alpha} > 0$) will have the same expression if it is gyroscopically stable ($s_g > 1$). $\dot{\phi}_{1R}$ and $\dot{\phi}_{2R}$ are both positive, but $\dot{\phi}_{1R}$ is still larger than $\dot{\phi}_{2R}$.

For a nonspinning statically stable missile,

$$\dot{\phi}_{1R} = -\dot{\phi}_{2R} = \omega_R \ , \tag{25}$$

where

$$\omega_R = \sqrt{\left(g_1 d / I_t\right)\left|C_{M\alpha}\right|} \ . \tag{26}$$

The frequencies for a statically unstable missile with gyroscopic stability factor equal to 1 have a similar form.

$$\dot{\phi}_{1R} = \dot{\phi}_{2R} = \omega_R \ . \tag{27}$$

The elastic motion of a homogeneous circular rod with constant diameter is determined by its fineness ratio *L*. and an elastic parameter ω_0^2.

$$\omega_0^2 = E_0 I_0 L / m d^3 \ . \tag{28}$$

E_0 is Young's modulus at the center of the rod and I_0 is the area moment of inertia at the center of the rod. The standard analysis for a nonspinning free-free beam gives the following relation for infinity of elastic frequencies:

$$\omega_K = \left(f_K / L\right)^2 \omega_0 \ , \tag{29}$$

where

$$f_K = 4.730, 7.853, 10.996, 14.137... \ . \tag{30}$$

For the odd number modes, the rod is symmetric U-shaped, whereas for the even number modes, the rod is antisymmetric S-shaped.

In Murphy and Mermagen (*6*), the parameter $\sigma = \omega_1 / \omega_R$ was used as a measure of the elasticity of a finned missile. We will continue to use this parameter to describe the elasticity of a spin-stabilized projectile. For a slowing spinning finned projectile, it has been shown that the aerodynamic frequencies are affected by the elasticity when $\sigma < 20$. For a spin-stabilized projectile, the first elastic frequency should be compared with the spin and not the aerodynamic frequency. Thus, we will see that the elastic frequencies are affected by the spin when $\sigma < 200$.

The frequencies present in the motion of a nonspinning elastic projectile would form an infinite sequence where the first two frequencies would be related to $\dot{\phi}_{1R}$ and $\dot{\phi}_{2R}$, while the later ones would evolve from $\pm\omega_K$, i.e., $\left(\dot{\phi}_{2K+1} \cong \omega_K ; \dot{\phi}_{2K+2} \cong -\omega_K \text{ for } \sigma \geq 200\right)$. The odd-numbered modes

rotate in the direction of the spin, have positive frequencies, and are called positive modes, while the even-numbered modes have negative frequencies and are called negative modes. Since the modes for a spinning missile essentially bifurcate, $j = 3$ is a symmetric mode rotating in the direction of spin, $j = 4$ is a symmetric mode rotating in an opposite direction to the spin, $j = 5$ is an antisymmetric mode rotating in the direction of spin, $j = 6$ is an antisymmetric mode rotating against the direction of spin, etc.

5. FEM

The rod is assumed to be represented by the sum of an inelastic bent component rotating with the missile and an elastic deformation.

$$\delta_E(x,t) = \delta_{EB}(x)e^{i\phi} + \tilde{\delta}_E(x,t); \qquad x_1 \le x \le x_2, \tag{31}$$

and

$$\delta_b(x,t) = \delta_{EB}(x) + \tilde{\delta}_b(x,t); \qquad x_1 \le x \le x_2, \tag{32}$$

where

$$\delta_{EB}(0) = \frac{d\delta_{EB}(0)}{dx} = 0. \tag{33}$$

Because the aerodynamic nose structure is rigidly attached to the rod,

$$\delta_E(x,t) = \delta_E(x_2,t) + (x - x_2)\Gamma(x_2,t) \qquad x_2 \le x \le x_3. \tag{34}$$

The motion of the elastic component of the rod is controlled by the elasticity of the rod and the aerodynamic force acting on it.

FEM is a very powerful method for calculating the time history of the elastic flexing motion. The rod is divided into n_j elements of length $L_e = L/n_j$. We will consider only an odd number of elements with the center of the central element satisfying equation 2.

The shape of the j-th element is given by a linear combination of third-order Hermitian polynomials (*6*).

$$\tilde{\delta}_b(x,t) = \sum_1^4 \hat{q}_{bp}(t)N_p(z), \tag{35}$$

where

$$x = L_e(z + z_j), \tag{36}$$

$$z_j = x_1/L_e + j - 1, \tag{37}$$

and

$$0 \le z \le 1. \tag{38}$$

The coefficients of the polynomials are complex functions of time and are called connectors. The first two connectors are the deflection and slope of the left end of the element and the third and fourth are the deflection and slope of the right end. To ensure continuity in deflection and slope at junction points, the corresponding pairs of connectors are equal. For n_j elements, there are $2n_j$ independent complex connectors, q_n. It is convenient to let the index for the connectors run from 3 to $n_t = 2n_j + 2$.

In Murphy and Mermagen (*6*), n_t complex second-order differential equations are derived for the n_t complex variables q_n.

$$\sum_{n=1}^{n_t}\left[R_{mn}\ddot{q}_n + \left(S_{mn} + i\dot{\phi}S^*_{mn}\right)\dot{q}_n + \left(T_{mn} + i\dot{\phi}T^*_{mn}\right)q_n \right] = t_m e^{i\phi}, \tag{39}$$

where

$$q_n = \left(q_{bny} + iq_{bnz}n\right)e^{i\phi} \tag{40}$$

and

$$t_m = \left(md^2\right)t_{mD} + \left(g_1 d\right)t_{mA}. \tag{41}$$

The $7n_t$ coefficients in equation 41 are defined for no Magnus force in Murphy and Mermagen (*6*). The inclusion of the Magnus force distribution function, $c_{fM}(x)$, modifies some of the T^*_{mn} and t_{mA} coefficients in appendix C.

6. Cone Cylinder Frequencies

Transient frequencies and damping rates for a 9-cal. cylindrical rod with a 1-cal. conical nose can be obtained from the homogeneous part of equations 41, ($t_m = 0$). The necessary parameters are given in appendix D. The first eight frequencies and damping rates for $\sigma = 20$ were obtained from 3-, 5-, and 7-element codes and are compared with results of the PDE method of Murphy and Mermagen (*5*) (table 1). The frequencies that differ from PDE results by >5% are marked by a "x." The 3-element code gives good results for the first four frequencies and the 5-element code is good for the sixth, seventh, and eighth frequencies. The fifth frequency, however, requires more than seven elements. In figure 3, the rod shapes for the fifth mode are plotted for the FEM code and the PDE value. We see that the antisymmetric shape specified by the PDE value probably requires at least 13 segments to describe it.

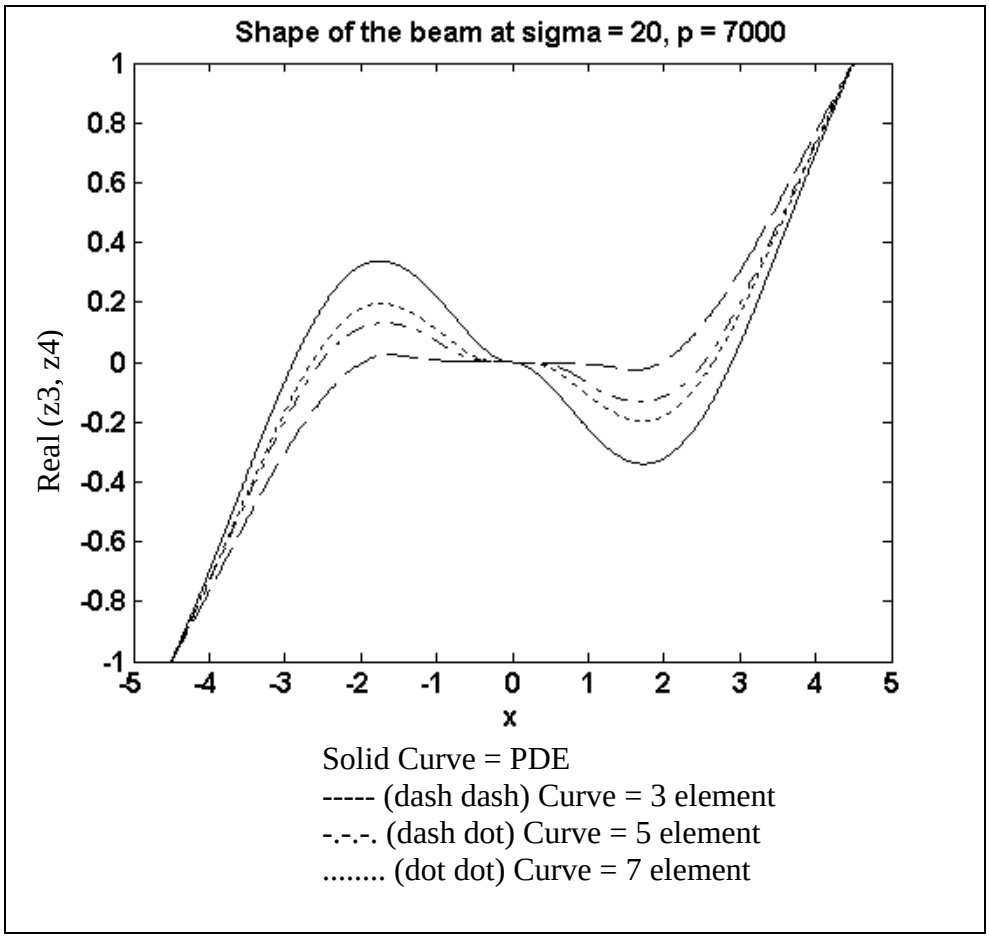

Figure 3. Shape of the beam for j = 3, 5, 7 element and PDE (real part of the shape).

The two aerodynamic frequencies do not differ from their rigid values. The elastic frequencies, however, are quite different from nonspinning values of $\pm\omega_K$. The first two positive frequencies are 150% and 130% greater than these values.

Figure 4 shows the positive and negative first elastic frequencies divided by the zero-spin value given by equation 30. When the first elastic frequency is much greater than the spin ($\sigma \approx 200$), these ratios are near unity. Figure 5 shows similar results for positive and negative second elastic frequencies.

7. Bent Projectile Resonances

In Murphy and Mermagen (*5*, *6*), a bent rod was described by a pair of quartic curves:

$$\begin{aligned} \delta_{EB} &= d_{11}x^2 + d_{21}x^4 \qquad -L/2 \le x \le 0 \\ &= d_{12}x^2 + d_{22}x^4 \qquad 0 \le x \le L/2. \end{aligned} \tag{42}$$

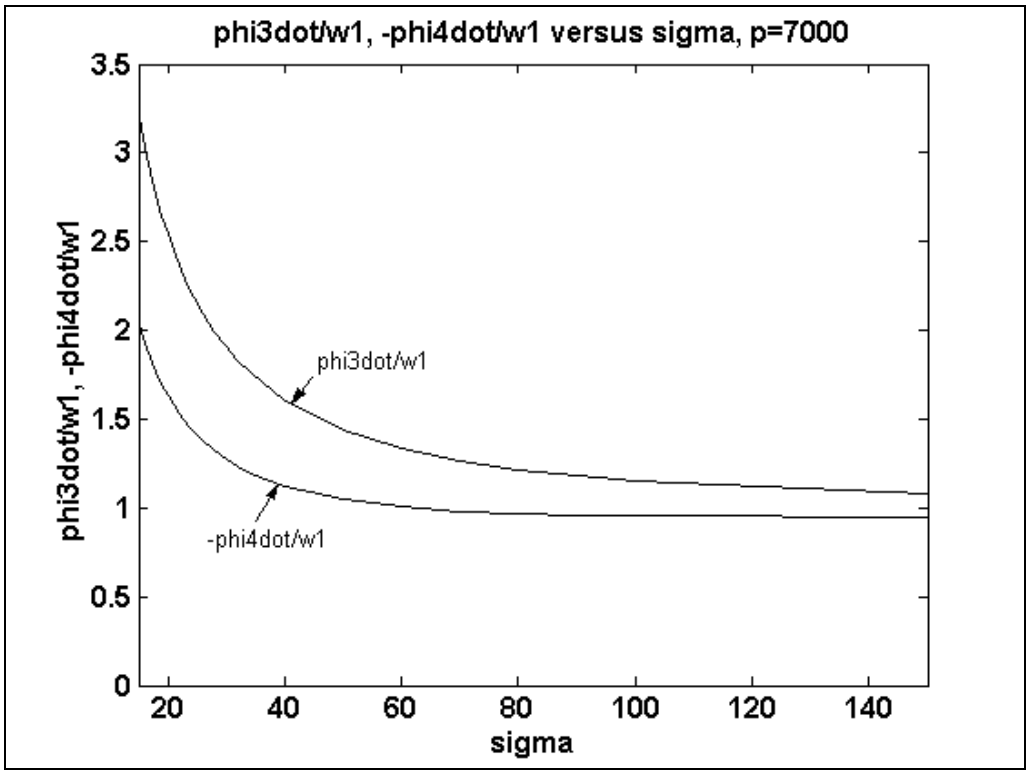

Figure 4. $\dot{\phi}_3/\omega_1, -\dot{\phi}_4/\omega_1$ vs. σ.

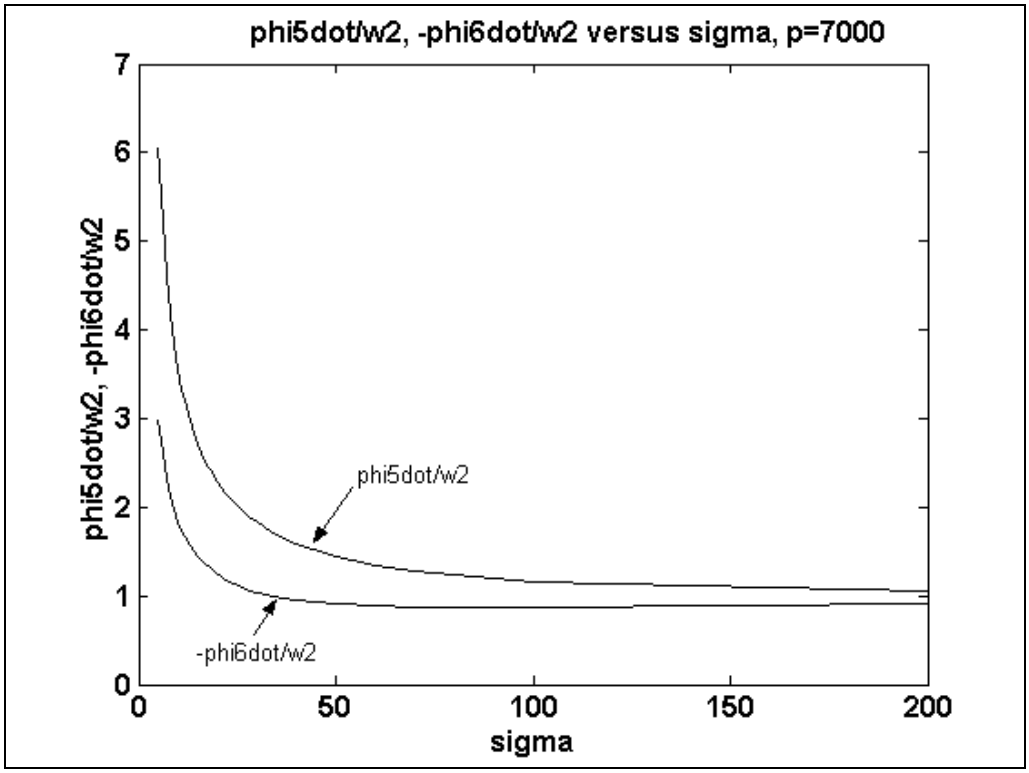

Figure 5. $\dot{\phi}_5/\omega_2, -\dot{\phi}_6/\omega_2$ vs. σ.

These curves can then be used to calculate the inhomogeneous coefficients in equation 42. For a slowly spinning finned missile, the aerodynamic coefficients, t_{mA}, dominate while for a rapidly spinning projectile the dynamic coefficients, t_{mD}, dominate. These inhomogeneous terms induce a modal response at the spin frequency that can have a large amplitude when the spin is equal to one of the transient frequencies. The values of d_{ij} given in appendix D specify the very small deflection of the rod forward tip of 0.0015 in.

For constant spin, special solutions of equation 39 have been calculated in Murphy and Mermagen (*6*). These trim solutions have the form

$$q_n(t) = s_n e^{i\dot{\phi}t} . \tag{43}$$

Using 5 elements, the 12 s_n's can be computed for fixed values of spin and σ. The complex location of the forward end of the rod is specified by s_{11}.

In figure 6, the amplitude of the forced motion of the forward end of the rod is plotted vs. σ for two values of spin. The resonances at $\sigma = 119.3, 126.3$ occur when the positive first elastic frequency is equal to a spin value while the resonances at $\sigma = 21.9, 23.2$ occur when the positive second elastic frequency is equal to a spin value. The amplitude of the flexing motion of the forward end of the rod is 70% of its diameter.

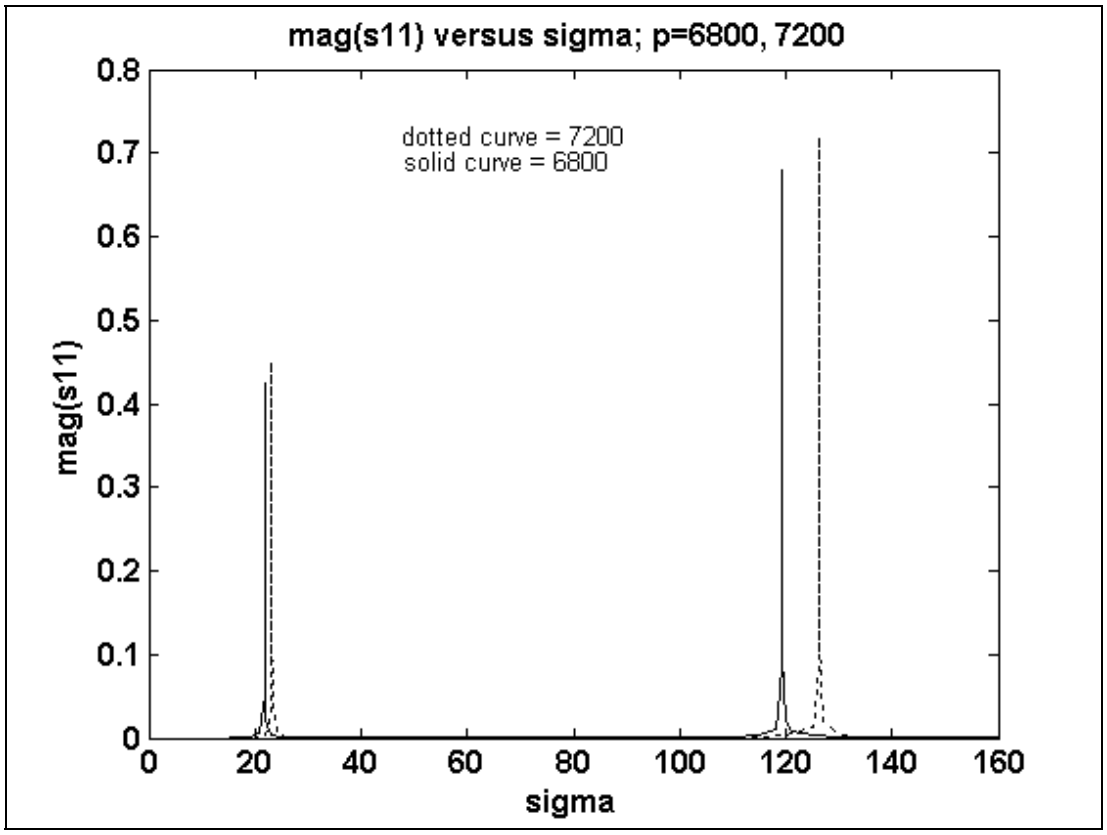

Figure 6. $mag(s_{11})$ vs. σ for 5-element code, $\dot{\phi}$ = 7200 rad/s, 6800 rad/s.

In Murphy and Mermagen (*6*), a nonlinear spin equation is derived:

$$I_X\ddot{\phi} + Re\left\{md^2\left(Q_D - i\dot{q}_2\bar{J}_6 + iq_2\bar{J}_8\right) - g_1 d\, Q_A\right\} = g_1 d\left(C_l\right)_{linear}, \tag{44}$$

where the cubic terms I_X, Q_D, J_8, and Q_A are defined.

For a cone cylinder, the linear roll moment coefficient has a very simple form,

$$\left(C_l\right)_{linear} = C_{l_p}\left(\dot{\phi}d/V\right). \tag{45}$$

Equations 39 and 44 for five elements can be integrated to show the occurrence of resonance with the positive first elastic frequency ($\sigma = 122.8$). All initial conditions are made zero except for $\dot{\phi}_0$ = 7000 rad/s. Figures 7–9 show the time variation of spin, angle of attack magnitude, and rod forward tip motion magnitude, $\dot{\phi}, |q_{1b}|, |q_{11b}|$. Resonance is clearly shown at t = 0.25 s when spin is near 7000 rad/s. According to figure 9, the maximum amplitude of the forward rod motion is 30% of the rod diameter. Thus, the motion amplification due to spin going through resonance is less than half its resonance value. For rigid finned projectiles, relations between pitching motion amplitude due to spin varying through resonance and its resonance value are given in Murphy (*8*).

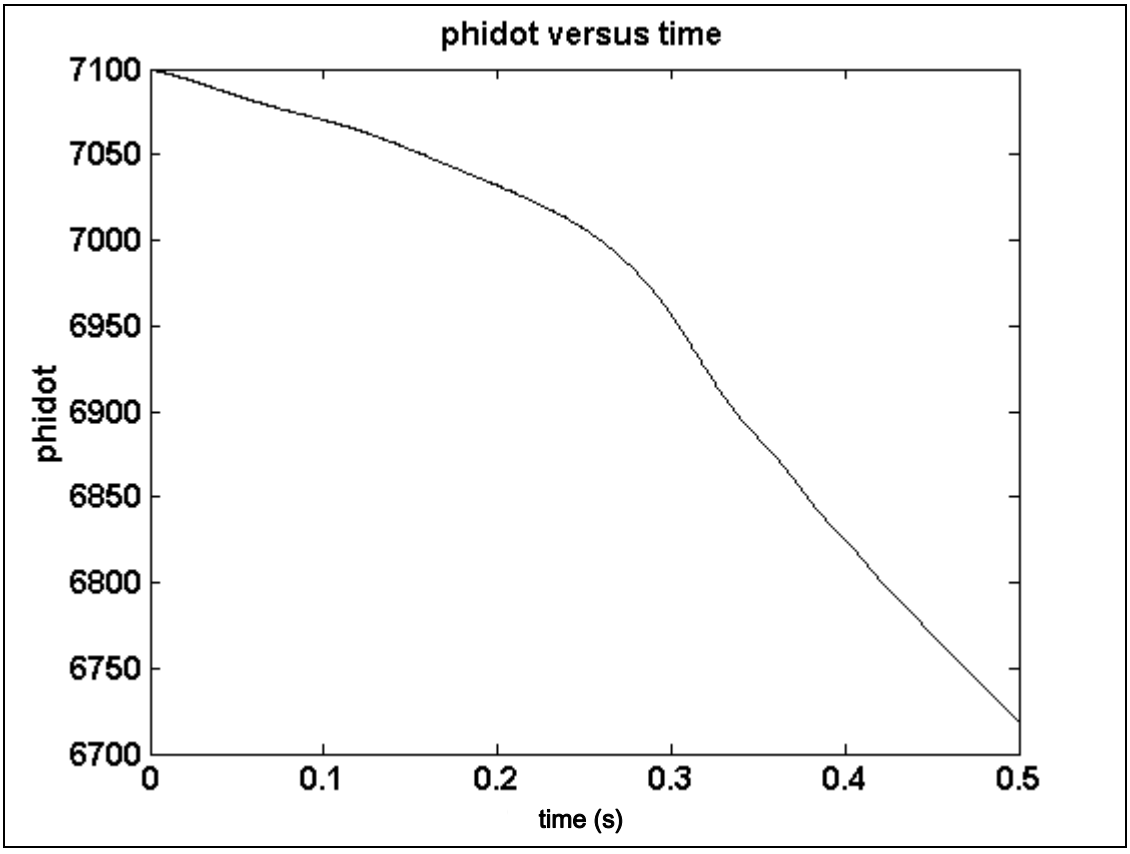

Figure 7. $\dot{\phi}$ vs. time for σ = 122.8, $\dot{\phi}_0$ = 7100.

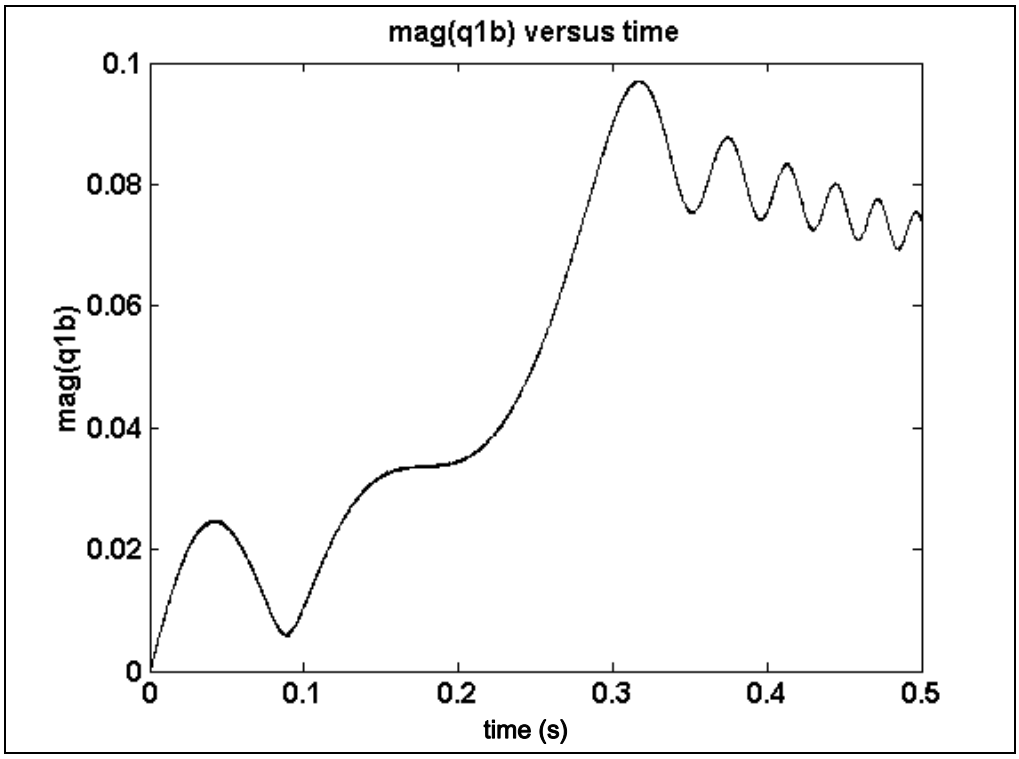

Figure 8. $mag\left(q_{1b}\right)$ vs. time for σ = 122.8, $\dot{\phi}_0$ = 7100.

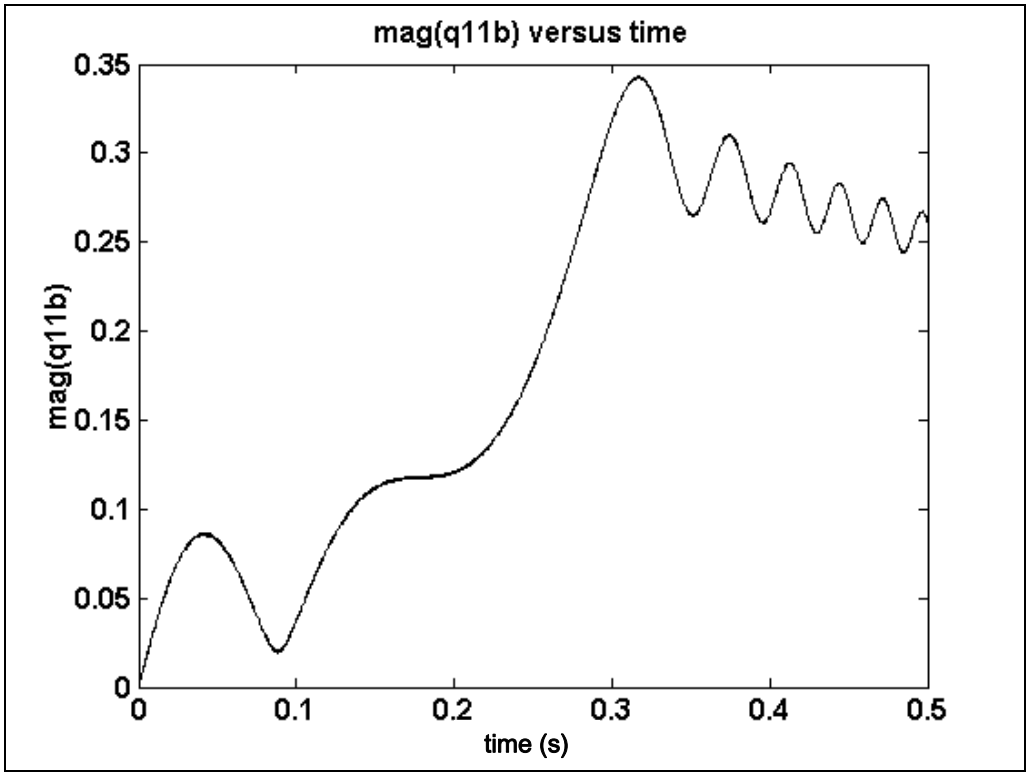

Figure 9. $mag\left(q_{11b}\right)$ vs. time for σ = 122.8, $\dot{\phi}_0$ = 7100.

For the symmetric waveform of the first elastic mode for a nonspinning rod with no force loading, the maximum strain occurs at the midpoint.

$$\varepsilon_M = (1/2)\left|\frac{\partial^2 \delta_E(0)}{\partial x^2}\right|. \tag{46}$$

Figure 10 shows the variation of maximum strain with time. For most metals, yield occurs for strain >0.0015. Thus, figure 10 shows yield at resonance.

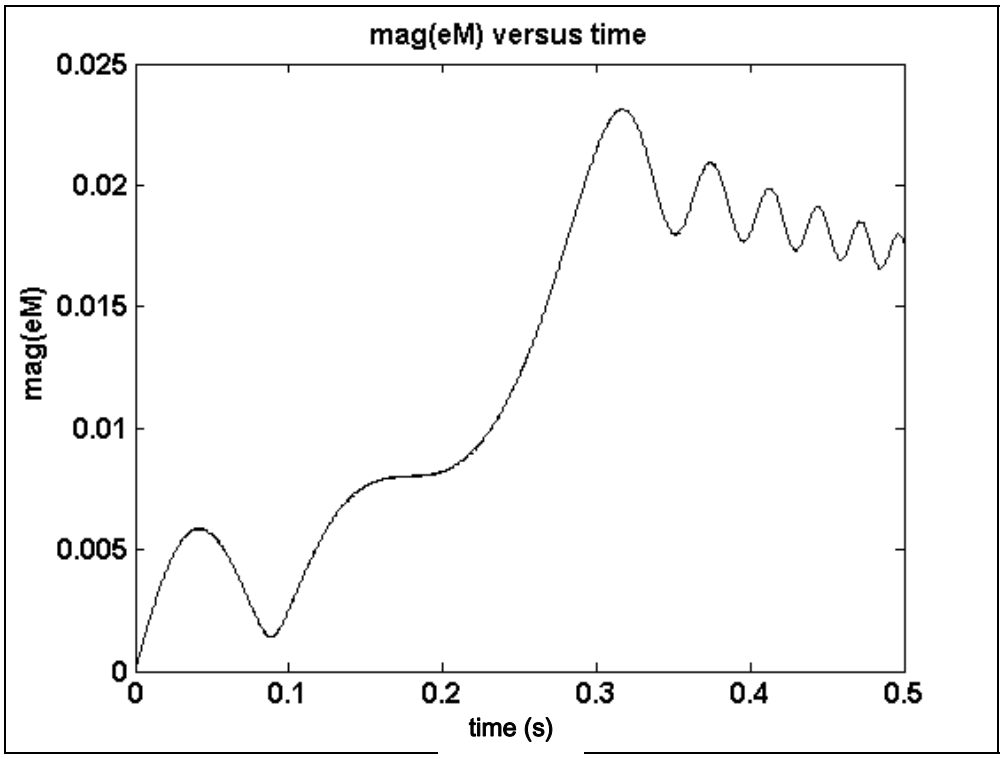

Figure 10. mag (e_M) vs. time for σ = 122.8, $\dot{\phi}_0$ = 7100.

8. Summary

The previously derived FEM theory, which was applied to slowly spinning finned projectiles, has been extended to rapidly spinning spin-stabilized projectiles.

Positive and negative elastic frequencies for a spin-stabilized projectile have been calculated, and their magnitudes have been shown to be significantly different for $\sigma < 200$.

Resonance with the first elastic mode has been demonstrated, and very small rigid asymmetries have been shown to cause yield at resonance.

9. References

1. Platus, D. H. Aero Elastic Stability of Slender, Spinning Missiles. *Journal of Guidance, Control and Dynamics* **January–February 1992**, *15*, 144–151.

2. Legner, H. H.; Lo, E. Y.; Reinecke, W. G. *On the Trajectory of Hypersonic Projectiles Undergoing Geometry Changes*, AIAA Aerospace Sciences Meeting, Reno, NV, 10–13 January 1994; AIAA 94-0719.

3. Heddadj, S.; Cayzac, R.; Renard, J. *Aeroelasticity of High L/D Supersonic Bodies: Theoretical and Numerical Approach*, AIAA Aerospace Sciences Meeting, Reno, NV, 10–13 January 2000; AIAA 2000-0390.

4. Murphy, C. H.; Mermagen, W. H. Flight Mechanics of an Elastic Symmetric Projectile. *Journal of Guidance, Control and Dynamics* **November–December 2001**, *24*, 1125–1132.

5. Murphy, C. H.; Mermagen, W. H. Flight Motion of a Continuously Elastic Finned Missile. *Journal of Guidance, Control and Dynamics* **January–February 2003**, *26*, 89–98.

6. Murphy, C. H.; Mermagen, W. H. *Spin-Yaw Lockin of an Elastic Finned Projectile*; ARL-TR-3217; U.S. Army Research Laboratory: Aberdeen Proving Ground, MD, August 2004.

7. Geradin, M.; Rixen, D. *Mechanical Vibrations: Theory and Applications to Structural Dynamics*; John Wiley: Chichester, 1994.

8. Murphy, C. H. *Response of an Asymmetric Missile to Spin Varying Through Resonance*; BRL-1545; U.S. Army Ballistic Research Laboratory: Aberdeen Proving Ground, MD, July 1971.

INTENTIONALLY LEFT BLANK.

Appendix A. Improved Partial Differential Equation

The roll moment of inertia of a circular disk is $2a_d\left(md^2\right)\rho_2(x)dx$ and its transverse moment of inertia is $a_d\left(md^2\right)\rho_2(x)dx$ where a_d is $(16L)^{-1}$ and $\rho_2(x)$ describes the variation of moments of inertia along rod. In the derivation of the partial differential equation (PDE) in Murphy and Mermagen,[1] the disks were assumed to be point masses, i.e., $a_d = 0$. In Murphy and Mermagen,[2] the kinetic energy associated with a_d for a disk was shown to be $T_{ad}dx$, where

$$T_{ad} = \left(a_d md^2/2\right)\left[\dot{\Gamma}_y^2 + \dot{\Gamma}_z^2 + 2\,\mathrm{Re}\left\{\dot{\phi}\left(2i\dot{\Gamma} - \dot{\phi}\Gamma\right)\overline{\Gamma} + i\left(\dot{\Gamma} - 2i\dot{\phi}\Gamma\right)\overline{Q}\right\}\right]\rho_2, \tag{A-1}$$

where $Q = i\dot{q}_{1e}$.

According to Geradin and Rixen,[3] two terms in T_{ad} appear in the PDE for a flexing projectile:

$$\frac{d}{dt}\left(\frac{\partial T_{ad}}{\partial \dot{\Gamma}_y}\right) - \left(\frac{\partial T_{ad}}{\partial \Gamma_y}\right) = \left(md^2 a_d\right)\left[\ddot{\Gamma}_y + 4\dot{\phi}\dot{\Gamma}_z + 2\dot{\phi}^2\Gamma_y + \dot{r} - 2\dot{\phi}q\right], \tag{A-2}$$

and

$$\frac{d}{dt}\left(\frac{\partial T_{ad}}{\partial \dot{\Gamma}_z}\right) - \left(\frac{\partial T_{ad}}{\partial \Gamma_z}\right) = \left(md^2 a_d\right)\left[\ddot{\Gamma}_z - 4\dot{\phi}\dot{\Gamma}_y + 2\dot{\phi}^2\Gamma_z - \dot{q} - 2\dot{\phi}r\right]. \tag{A-3}$$

The contribution of $\tilde{T}_d$ to the improved PDE is obtained by multiplying the second term by i, adding it to the first term and differentiating the result with respect to x. The improved version of equation 52 in Murphy and Mermagen[1] is

$$\begin{aligned}
&\frac{\partial^2 \delta_E}{\partial t^2} + \omega_0^2 \frac{\partial^4 \delta_E}{\partial x^4} + \omega_0^2 \hat{k}\, c_{d4} \\
&\quad - g_2\left[L\left(c_{f1} + i\left(pd/V\right)c_{fM}\right)\Gamma + \left(c_{f2}\dot{\Gamma} - c_{f1}\dot{\delta}_E\right)\left(d/V\right) - \frac{\partial\left(c_D\delta\right)}{\partial x}\right] \\
&\quad = a_d L\frac{\partial}{\partial x}\left(\ddot{\Gamma} - 4i\dot{\phi}\dot{\Gamma} + 2\dot{\phi}^2\Gamma\right) + E_1\xi + E_2\dot{\xi} + ix\dot{Q} - N.
\end{aligned} \tag{A-4}$$

[1] Murphy, C. H.; Mermagen, W. H. Flight Motion of a Continuously Elastic Finned Missile. *Journal of Guidance, Control and Dynamics* **January–February 2003**, *26*, 89–98.

[2] Murphy, C. H.; Mermagen, W. H. *Spin-Yaw Lockin of an Elastic Finned Projectile*; ARL-TR-3217; U.S. Army Research Laboratory: Aberdeen Proving Ground, MD, August 2004.

[3] Geradin, M.; Rixen, D. *Mechanical Vibrations: Theory and Applications to Structural Dynamics*; John Wiley: Chichester, 1994, pp 172–174.

The first boundary conditions at x_1 and x_2 are modified by adding the sum of the first term and i times the second term evaluated at x_1 and x_2. Equations 53 and 55 of Murphy and Mermagen[1] become

$$\frac{\partial^3 \delta_E(x_1,t)}{\partial x^3} + \hat{k} c_{d3}(x_1,t) + g_4 c_D(x_1)\delta(x_1,t) + a_d L\left[i\dot{Q} - \left(\ddot{\Gamma}(x_1,t) + 2\dot{\phi}^2 \Gamma(x_1,t)\right) - 2i\dot{\phi}\left(iQ - 2\dot{\Gamma}(x_1,t)\right)\right]\omega_0^{-2} = -g_4 f_1 \quad \text{(A-5)}$$

and

$$\frac{\partial^3 \delta_E(x_2,t)}{\partial x^3} + \hat{k} c_{d3}(x_2,t) + g_4 c_D(x_2)\delta(x_2,t) + a_d L\left[i\dot{Q} - \left(\ddot{\Gamma}(x_2,t) + 2\dot{\phi}^2 \Gamma(x_2,t)\right) - 2i\dot{\phi}\left(iQ - 2\dot{\Gamma}(x_2,t)\right)\right]\omega_0^{-2} = g_4 f_2. \quad \text{(A-6)}$$

The trim solution equations 78, 79, 81, 86, and 87 of Murphy and Mermagen[1] are replaced by

$$\frac{d^4\tilde{\delta}_{ET}}{dx^4} - E_6\frac{d^2\tilde{\delta}_{ET}}{dx^2} - E_4\frac{d\tilde{\delta}_{ET}}{dx} + E_5\tilde{\delta}_{ET} - g_4\tilde{\delta}_{Tc}\frac{dc_D}{dx} = E_3\xi_T - N_T^* - E_{BF}^* + E_B, \quad \text{(A-7)}$$

$$\frac{d^3\tilde{\delta}_{ET}(x_1)}{dx^3} + g_4 c_D(x_1)\delta_T(x_1) + E_6\left[(\xi_T/5) - \Gamma_T(x_1)\right] - ia_d\left(\dot{\phi}d/V\right)\left[g_4 C_{L\alpha}\xi_T - LN_T\omega_0^{-2}\right] = -g_4 f_{1T}, \quad \text{(A-8)}$$

$$\frac{d^3\tilde{\delta}_{ET}(x_2)}{dx^3} + g_4 c_D(x_2)\delta_T(x_2) + E_6\left[(\xi_T/5) - \Gamma_T(x_2)\right] - ia_d\left(\dot{\phi}d/V\right)\left[g_4 C_{L\alpha}\xi_T - LN_T\omega_0^{-2}\right] = g_4 f_{2T}, \quad \text{(A-9)}$$

$$\frac{d^4 w_1}{dx^4} - E_6\frac{d^2 w_1}{dx^2} - E_4\frac{dw_1}{dx} + E_5 w_1 = E_3\xi_T - N_T^* - E_{BF}^* + E_B + g_4\tilde{\delta}_{cT}\frac{dc_D}{dx}, \quad \text{(A-10)}$$

and

$$\frac{d^4 w_m}{dx^4} - E_{\wedge}\frac{d^2 w_m}{dx^2} - E_4\frac{dw_m}{dx} + E_5 w_m = 0; \qquad m = 2, 3, \quad \text{(A-11)}$$

where

$$E_4 = g_4\left[c_{f1} + \left(i\dot{\phi}d/V\right)\left(c_{f2} + c_{fM}\right) - c_D\right], \quad \text{(A-12)}$$

$$E_6 = 5a_d L\dot{\phi}^2\omega_0^{-2}, \quad \text{(A-13)}$$

and

$$E_B = g_4\left[\left(c_{f1} + i\left(\dot{\phi}d/V\right)c_{fM}\right)\Gamma_B + \left(c_{f2}\Gamma_B - c_{f1}\delta_{EB}\right)\left(i\dot{\phi}d/V\right) - \frac{d\left(c_D\delta_{EB}\right)}{dx}\right]$$
$$+\left(\dot{\phi}/\omega_0\right)^2\delta_B + E_6\frac{d\Gamma_B}{dx}\ . \tag{A-14}$$

The transient solution equations 92, 94–96, and 98 of Murphy and Mermagen[1] are replaced by

$$b_3\frac{d^4\psi_k}{dx^4} - E_{6k}\frac{d^2\psi_k}{dx^2} - E_{4k}\frac{d\psi_k}{dx} + E_{5k}\psi_k - g_4\psi_{kc}\frac{dc_D}{dx} = E_{3k} - N_k^*, \tag{A-15}$$

$$b_3\frac{d^4w_4}{dx^4} - E_{6k}\frac{d^2w_4}{dx^2} - E_{4k}\frac{dw_4}{dx} + E_{5k}w_4 = E_{3k} - N_k^* + g_4\psi_{kc}\frac{dc_D}{dx}, \tag{A-16}$$

$$b_3\frac{d^4w_m}{dx^4} - E_{6k}\frac{d^2w_m}{dx^2} - E_{4k}\frac{dw_m}{dx} + E_{5k}w_m = 0 \quad ; \quad m = 5,6, \tag{A-17}$$

$$\frac{d^3\psi_k}{dx^3} + g_4E_{7k}^{-1}c_D\left(\psi_k - \psi_{kc}\right) + b_3^{-1}\left[E_{7k} - E_{6k}\frac{d\psi\left(x_1\right)}{dx}\right]$$
$$+a_d\left(A_k - 2i\dot{\phi}\right)\left(d/V\right)\left[g_4C_{L\alpha} - LN_k\omega_0^{-2}\right]b_3^{-1} = -g_4E_{7k}^{-1}f_{1k}, \tag{A-18}$$

and

$$\frac{d^3\psi_k}{dx^3} + g_4E_{7k}^{-1}c_D\left(\psi_k - \psi_{kc}\right) + b_3^{-1}\left[E_{7k} - E_{6k}\frac{d\psi\left(x_2\right)}{dx}\right]$$
$$+a_d\left(A_k - 2i\dot{\phi}\right)\left(d/V\right)\left[g_4C_{L\alpha} - LN_k\omega_0^{-2}\right]b_3^{-1} = g_4E_{7k}^{-1}f_{2k}, \tag{A-19}$$

where

$$E_{6k} = a_dL\left(A_k^2 - 4i\dot{\phi}A_k + 2\dot{\phi}^2\right)\omega_0^{-2}, \tag{A-20}$$

$$E_{7k} = a_dLA_k\left(A_k - 2i\dot{\phi}\right)\omega_0^{-2}, \tag{A-21}$$

and

$$b_3 = 1 + 2\hat{k}\omega_1^{-1}\left(A_k - i\dot{\phi}\right). \tag{A-22}$$

For simplicity, the small Magnus contribution to the boundary conditions in this appendix have been neglected.

INTENTIONALLY LEFT BLANK.

Appendix B. Integrals

B.1 Aerodynamic Coefficents

$$c_1 = \int_{x_0}^{x_3} c_{f1}\,dx = C_{N\alpha} \qquad c_3 = \int_{x_0}^{x_3} c_{f1}\,x\,dx = \left[C_{M\alpha}\right]_0$$

$$c_{1M} = \int_{x_0}^{x_3} c_{fM}\,dx = C_{Np\alpha} \qquad c_{3M} = \int_{x_0}^{x_3} c_{fM}\,x\,dx = \left[C_{Mp\alpha}\right]_0$$

$$c_2 = \int_{x_0}^{x_3} c_{f3}\,dx = \left[C_{Nq} + C_{N\dot{\alpha}}\right]_0 \qquad c_4 = \int_{x_0}^{x_3} c_{f3}\,x\,dx = \left[C_{Mq} + C_{M\dot{\alpha}}\right]_0$$

$$c_{f3} = 2c_{f2} - xc_{f1} \qquad \left[\quad\right]_0 \Rightarrow x_c = 0$$

B.2 Functions of Time

$$\delta_c(t) = (1/L)\int_{x_1}^{x_2} \delta_E \rho_1\,dx \qquad J_3(t) = \int_{x_0}^{x_3} c_{f1}\Gamma\,x\,dx$$

$$J_1(t) = \int_{x_0}^{x_3} c_{f1}\Gamma\,dx \qquad J_{3M}(t) = \int_{x_0}^{x_3} c_{fM}\Gamma\,x\,dx$$

$$J_{1M}(t) = \int_{x_0}^{x_3} c_{fM}\Gamma\,dx \qquad J_4(t) = \int_{x_0}^{x_3} \left(c_{f2}\Gamma - c_{f1}\delta_E\right)x\,dx$$

$$J_2(t) = \int_{x_0}^{x_3} \left(c_{f2}\Gamma - c_{f1}\delta_E\right)dx \qquad J_5(t) = \int_{x_0}^{x_3} c_D\left(\delta_E - \delta_c\right)dx + \left[\delta_E(x_1) - \delta_c\right]C_{Dbp}$$

INTENTIONALLY LEFT BLANK.

Appendix C. Magnus Terms

$$c_{1M} = C_{N p\alpha} = \int_{x_0}^{x_3} c_{fM}(x)\,dx \qquad c_{3M} = C_{M p\alpha} = \int_{x_0}^{x_3} c_{fM}(x)\,x\,dx$$

$$J_{1MB} = \int_{x_0}^{x_3} c_{fM}\Gamma_B\,dx \qquad J_{3MB} = \int_{x_0}^{x_3} c_{fM}\Gamma_B\,x\,dx$$

$$\hat{h}^1_{qj} = \int_0^1 c_{fM}(x)\,N'_q(z)\,dz \qquad x = L_e(z_j + z)$$

$$\hat{h}^2_{qj} = \int_0^1 \left[c_{fM}(x)\,N'_q(z)\right] x\,dz \qquad z_j = (x_1/L_e) + j - 1$$

$$\hat{h}_{pj1} = L_e \int_0^1 c_{fM}(x)\,N_p(z)\,dz \qquad p,q = 1,2,3,4$$

$$\hat{h}_{Bpj} = L_e \int_0^1 c_{fM}\Gamma_B N_p\,dz$$

$\hat{h}^1_{qc}, \hat{h}^1_{qa}, \hat{h}^2_{qa}, \hat{h}^2_{qc}, \hat{h}_{pc1}, \hat{h}_{pa1}, \hat{h}_{Bpc}, \hat{h}_{Bpa}$ are calculated from $\hat{h}^1_{qj}, \hat{h}^2_{qj}, \hat{h}_{pj1}, \hat{h}_{Bpj}$ in the same manner as $\overleftarrow{f}_{pc}, \overleftarrow{f}_{pa}$ were computed from $\overleftarrow{f}_{pj}$.
$h_{1n}, h_{2n}, h_{m1}, h_{Bm}$ are then computed in the same way as f_m.

$$\hat{h}_{pqj} = \int_0^1 c_{fM}(x)\,N'_q(z)\,N_p(z)\,dz \qquad x = L_e(z_j + z)$$

$$z_j = (x_1/L_e) + j - 1$$

$$p,q = 1,2,3,4$$

h_{mn} is computed from $\hat{h}_{pqj}$ in the same manner as f_{mn} was computed from $\hat{f}_{pqj}$.
$m,n \geq 3$.

$$T_{11}^{*} = \left(g_1 d^2/V\right) c_{1M}$$
$$T_{21}^{*} = -\left(g_1 d^2/V\right) c_{3M}$$
$$T_{22}^{*} = -I_X$$
$$T_{1n}^{*} = -\left(g_1 d^2/V\right) h_{1n}$$
$$T_{2n}^{*} = -\left(g_1 d^2/V\right) h_{2n}$$
$$T_{m1}^{*} = -\left(g_1 d^2/V\right) h_{m1}$$
$$T_{m2}^{*} = 2md^2 a_d b_{2m}$$
$$T_{mn}^{*} = -\left(g_1 d^2/V\right) h_{mn} - \left(md^2/L\right)\left(2\omega_0^2/\omega_1\right)\hat{k} c_{mn} \qquad m, n \geq 3$$

$$t_{1A} = J_{1B} + i\left(\dot{\phi} d/V\right)\left(J_{2B} + J_{1MB}\right)$$
$$t_{2A} = J_{3B} + i\left(\dot{\phi} d/V\right)\left(J_{4B} + J_{3MB}\right)$$
$$t_{mA} = f_{Bm} + f_{aBm} + i\left(\dot{\phi} d/V\right)\left(g_{Bm} + g_{aBm} + h_{Bm}\right) \qquad m \geq 3$$

The Magnus force on the aerodynamic extension has a small effect on the flexing motion and has been neglected in the previous relations.

Appendix D. Projectile Parameters

$\rho_1 = \rho_2 = \rho_3 = 1$ $\quad x_c = 0$

$L = 9$ $\quad V = 3000$ ft/s

d = 0.35 ft $\quad \rho = 0.002$ slugs/ft^3

$m = 1.60$ slug $\quad x_{01} = 0 \quad x_{23} = 1$

$I_x = 0.0245$ slug-ft^2

$I_t = 1.335$ slug-ft^2

$c_{f1} = 4(5.5 - x)$ $\quad 4.5 < x \le 5.5$

$= e^{2(x-5.5)}$ $\quad -4.5 < x \le 4.5$

$c_{f2} = 2(5.5 - x)^2$ $\quad 4.5 < x \le 5.5$

$= 2 + 0.5\left(1 - e^{2(x-5.5)}\right)$ $\quad -4.5 < x \le 4.5$

$c_{fM} = 0$ $\quad 2 < x \le 5.5$

$= -0.07$ $\quad -4.5 < x \le 2$

$c_D = (0.30)(5.5 - x)$ $\quad 4.5 < x \le 5.5$

$= 0$ $\quad x \le 4.5$

$c_{Dbp} = 0.14$ $\quad C_{\ell p} = -0.025$

$d_{12} = 2 \times 10^{-5}$ $\quad d_{22} = -1.25 \times 10^{-7}$

$\dot{\phi} = 7000$ rad/s $\quad d_{11} = d_{21} = 0$

$\omega_{1R} = 102.8$ rad/s $\quad \omega_{2R} = 25.6$ rad/s

$\omega_R = 51.3$ rad/s $\quad s_g = 1.6$

$C_{N\alpha} = 2.5$ $\quad C_{M\alpha} = 11.7$

$C_{Nq} + C_{N\dot{\alpha}} = 34$ $\quad C_{Mq} + C_{M\dot{\alpha}} = -50$

$C_{Np\alpha} = -0.5$ $\quad C_{Mp\alpha} = 1.1$

$$\sigma = 20 \qquad \dot{\phi}/\omega_R = 136 \qquad \omega_{R1}/\omega_R = 1.99 \qquad \omega_{R2}/\omega_R = .50$$
$$\omega_1/\omega_R = 20.0 \qquad \omega_2/\omega_R = 55.1 \qquad \omega_3/\omega_R = 108$$

Table D-1. Transient frequencies and damping rates.

Code	***k***	$\dot{\phi}_k/\omega_R$	λ_k/ω_R
3 element	1	2.003	–0.0074
5 element	1	2.002	–0.0074
7 element	1	2.003	–0.0074
PDE	1	1.993	–0.0075
3 element	2	0.502	–0.0263
5 element	2	0.502	–0.0263
7 element	2	0.502	–0.0263
PDE	2	0.505	–0.0265
3 element	3	51.25	–0.0113
5 element	3	50.91	–0.0168
7 element	3	50.85	–0.0167
PDE	3	50.71	–0.0112
3 element	4	–32.85	–0.0213
5 element	4	–32.76	–0.0139
7 element	4	–32.74	–0.0138
PDE	4	–32.67	–0.0139
3 element	5	138.61x	–0.0186
5 element	5	130.02x	–0.0274
7 element	5	125.93x	–0.0256
PDE	5	118.94	–0.0237
3 element	6	–70.48	–0.0305
5 element	6	–69.20	–0.0161
7 element	6	–68.57	–0.0159
PDE	6	–67.29	–0.0158
3 element	7	172.74x	–0.0271
5 element	7	161.55	–0.0255
7 element	7	160.45	–0.0245
PDE	7	159.76	–0.0326
3 element	8	–01.99x	–0.0164
5 element	8	–93.05	–0.0150
7 element	8	–92.62	–0.0148
PDE	8	–92.34	–0.0144

Note: PDE = partial differential equation.

List of Symbols, Abbreviations, and Acronyms

$c_{fj}(x)$	aerodynamic force distribution functions
d	maximum rod diameter
$E(x)$	Young's modulus
E_0	Young's modulus at rod center
F	$F_y + iF_z$ complex transverse aerodynamic force
a_d	$(16L)^{-1}$
g_1	$\rho V^2 S/2$
$I(x)$	$(d)^4 \iint y^2 dydz = (d)^4 \iint z^2 dydz$, area moment of rod
I_0	area moment at rod center
I_x	axial moment of inertia of projectile
I_{t0}	transverse moment of inertia of projectile about rod center
L	rod length/rod maximum diameter
L_e	L/n_j, dimensionless length of element
m	projectile mass
$p = \dot{\phi}$	spin
n_j	number of rod elements
n_t	$2n_j + 2$
q_1	$\beta + i\alpha$, complex angle of attack of central disk (nsc)
q_{1e}	$\psi - i\theta$ complex yaw and pitch of central disk (nsc)
q_2	$\dot{\psi} - i\dot{\theta}$ complex yaw and pitch rate of central disk (nsc)
q_n	$n = 3.4 \ldots n_t$ FEM connectors (nsc)
q_{bn}	$n = 3.4 \ldots n_t$ FEM connectors (bfc)

S	$\pi d^2/4$
V	magnitude of projectile velocity
x_1, x_2	location of beam ends
x_{01}, x_{23}	dimensionless length of fore and aft aerodynamic extensions
x_c	axial location of center of mass
α	angle of attack of central disk (nsc)
β	angle of sideslip of central disk (nsc)
Γ	$\frac{\partial \delta_E}{\partial x}$, complex cant of disk
ε_M	maximum strain of rod
δ_E	$\delta_{Ey} + i\delta_{Ez}$, lateral displacement of disk (nsc)
ϕ	roll angle
$\dot{\phi}_k$	frequency of k-th mode
λ_k	damping of k-th mode
ρ	air density
ρ_1	axial variation of mass
σ	ω_1/ω_R
ω_1	lowest elastic frequency of beam in vacuum
ω_R	rigid projectile frequency for $s_g = 0, 1$
$\vec{F} = \left(F_x, F_y, F_z\right)$	aerodynamic force exerted on missile (nsc)
$\vec{M} = \left(M_x, M_y, M_z\right)$	aerodynamic moment exerted on missile (nsc)
$Re\{z\}$	real part of z
$Im\{z\}$	imaginary part of z

Carat superscript denotes quantity for a single element.

Tilde superscript denotes elastic parameter for bent missile.

B subscript denotes parameter for bent projectile.

E subscript denotes an elastic coordinate parameter (nsc).

b subscript denotes an body-fixed coordinate parameter (bfc).

(bfc) body-fixed coordinates

(nsc) nonspinning coordinates

NO. OF COPIES ORGANIZATION

1 (PDF ONLY) DEFENSE TECHNICAL INFORMATION CTR
DTIC OCA
8725 JOHN J KINGMAN RD
STE 0944
FORT BELVOIR VA 22060-6218

1 US ARMY RSRCH DEV & ENGRG CMD
SYSTEMS OF SYSTEMS INTEGRATION
AMSRD SS T
6000 6TH ST STE 100
FORT BELVOIR VA 22060-5608

1 INST FOR ADVNCD TCHNLGY
THE UNIV OF TEXAS
AT AUSTIN
3925 W BRAKER LN STE 400
AUSTIN TX 78759-5316

1 US MILITARY ACADEMY
MATH SCI CTR EXCELLENCE
MADN MATH
THAYER HALL
WEST POINT NY 10996-1786

1 DIRECTOR
US ARMY RESEARCH LAB
IMNE ALC IMS
2800 POWDER MILL RD
ADELPHI MD 20783-1197

3 DIRECTOR
US ARMY RESEARCH LAB
AMSRD ARL CI OK TL
2800 POWDER MILL RD
ADELPHI MD 20783-1197

3 DIRECTOR
US ARMY RESEARCH LAB
AMSRD ARL CS IS T
2800 POWDER MILL RD
ADELPHI MD 20783-1197

NO. OF COPIES ORGANIZATION

ABERDEEN PROVING GROUND

1 DIR USARL
AMSRD ARL CI OK TP (BLDG 4600)

NO. OF COPIES	ORGANIZATION
1	COMMANDER US ARMY ARDEC TECHNICAL LIBRARY PICATINNY ARSENAL NJ 07806-5000
1	COMMANDER US NAVAL SURFACE WEAPONS WARFARE CENTER T PEPITONE MS MC K21 DAHLGREN VA 22448
1	TECHNICAL DIRECTOR US ARMY ARDEC AMSTA AR TD PICATINNY ARSENAL NJ 07806-5000
1	HQ USAMC PRNCPL DPTY FOR TECHLGY ALEXANDRIA VA 22333-0001
12	COMMANDER US ARMY ARDEC AET A C NG J GRAU S KAHN H HUDGINS M AMORUSO E BROWN B WONG W TOLEDO S CHUNG C LIVECCHIA G MALEJKO J WHYTE PICATINNY ARSENAL NJ 07806-5000
3	COMMANDER US ARMY ARDEC SMCAR CCH V B KONRAD E FENNELL T LOUZERIO PICATINNY ARSENAL NJ 07806-5000
4	COMMANDER US ARMY ARDEC SMCAR FSE A GRAF D LADD E ANDRICOPOULIS K CHEUNG PICATINNY ARSENAL NJ 07806-5000
6	COMMANDER US ARMY ARDEC SMCAR CCL D F PUZYCKI D CONWAY D DAVIS K HAYES M PINCAY W SCHUFF PICATINNY ARSENAL NJ 07806-5000
3	DIRECTOR US ARMY RESEARCH OFC G ANDERSON K CLARK T DOLIGOWSKI PO BOX 12211 RESEARCH TRIANGLE PARK NC 27709-2211
2	COMMANDER US NAVAL SURFC WEAPONS CTR CODE DK20 MOORE CODE DK20 DEVAN DAHLGREN VA 22448-5000
2	COMMANDER WHITE OAK LABORATORY US NSWC APPLIED MATH BR CODE R44 PRIOLO CODE R44 WARDLAW SILVER SPRING MD 20903-5000
1	COMMANDER US ARMY AVN AND MIS CMND AMSAM RD SS AT W WALKER REDSTONE ARSENAL AL 35898-5010

NO. OF
COPIES ORGANIZATION

4 COMMANDER
US AIR FORCE ARMAMENT LAB
AFATL FXA
B SIMPSON
G ASATE
R ABELGREN
G WINCHENBACK
EGLIN AFB FL 32542-5434

2 DIRECTOR
SANDIA NATIONAL LAB
W OBERKAMPF
W WOLFE
DIVISION 5800
ALBUQUERQUE NM 87185

1 DIRECTOR
LOS ALAMOS NATIONAL LAB
W HOGAN MS G770
LOS ALAMOS NM 87545

1 DIRECTOR
NASA AMES RESEARCH CTR
L SCHIFF MS 258 1
MOFFETT FIELD CA 94035

1 DIRECTOR
NASA LANGLEY RESEARCH CTR
M HEMSCH
LANGLEY STATION
HAMPTON VA 23665

1 MASSACHUSETTS INST OF TECH
DEPT OF AERONAUTICS AND
ASTRONAUTICS
E COVERT
77 MASSACHUSETTS AVE
CAMBRIDGE MA 02139

1 ARROW TECHLGY ASSOC INC
R WHYTE
PO BOX 4218
BURLINGTON VT 05401-4218

2 C H MURPHY
PO BOX 269
UPPER FALLS MD 21156

2 W H MERMAGEN
4149 U WAY
HAVRE DE GRACE MD 21078

NO. OF
COPIES ORGANIZATION

1 W STUREK
3500 CARSINWOOD DR
ABERDEEN MD 21001-1412

1 OREGON STATE UNIV
DEPT OF MECH ENGR
DR M COSTELLO
CORVALLIS OR 97331

ABERDEEN PROVING GROUND

4 COMMANDER
US ARMY ARDEC
SMCAR DSD T
R LIESKE
F MIRABELLE
J WHITESIDE
J MATTS
APG MD 21005

26 DIR USARL
AMSRD ARL CI H
C NIETUBICZ
AMSRD ARL HR SC
D SAVICK
AMSRD ARL SL BE
A MIKHAIL
AMSRD ARL WM
E SCHMIDT
AMSRD ARL WM B
A HORST
AMSRD ARL WM BA
W D AMICO
B DAVIS
T HAWKINS
AMSRD ARL WM BC
M BUNDY
G COOPER
W DRYSDALE
J GARNER
B GUIDOS
B OSKAY
P PLOSTINS
J SAHU
K SOENCKSEN
P WEINACHT
S WILKERSON
AMSRD ARL WM BD
T MINOR

NO. OF
COPIES ORGANIZATION

AMSRD ARL WM BF
H EDGE
AMSRD ARL WM T
B BURNS
AMSRD ARL WM TC
R COATES
W DE ROSSET
R MUDD
AMSRD ARL WM TD
E RAPACKI

NO. OF
COPIES ORGANIZATION

1 DEFENSE RESEARCH
ESTABLISHMENT VALCARTIER
DELIVERY SYSTEM DIVISION
A D DUPUIS
2459 PIE XI NORD
VAL BELAIR QUEBEC
CANADA